Available online at www.sciencedirect.com
ScienceDirect
Journal of Sound and Vibration 307 (2007) 639–661
JOURNAL OF SOUND AND VIBRATION
www.elsevier.com/locate/jsvi

MIMO adaptive vibration control of smart structures with quickly varying parameters: Neural networks vs classical control approach

Rajiv Kumar[a,*], S.P. Singh[b], H.N. Chandrawat[c]

[a]Department of Industrial Engineering, National Institute of Technology, Jalandhar-144011, Punjab, India
[b]Department of Mechanical Engineering, Indian Institute of Technology, Hause Khas, New Delhi-11016, India
[c]Department of Mechanical Engineering, Thapar Institute of Engineering and Technology, Patiala-147001, Punjab, India

Received 4 August 2006; received in revised form 20 June 2007; accepted 23 June 2007
Available online 30 August 2007

Abstract

This paper presents experimental adaptive identification and control of smart structures using neural networks based on system classification technique. An inverted L-structure with surface-bonded piezoceramic sensors/actuators is used for analysis. The state space, as well as matrix fraction description presentation, from control input voltages to output sensor voltage, is established in multivariable form. It is observed that the computational time required for online parameter identification and controller design is generally quite high. For the system, whose parameters change abruptly with large amplitudes, classical adaptive control techniques give poor transient behavior and sometimes instability. Also, for obtaining the ideal closed-loop performance, linear quadratic regulator cannot be re-designed in real-time for changed parameters of the smart structures, even if these parameters are identified in real time. Closed-loop identification of system parameters and control gains using system classification-based neural networks is proposed and implemented. A preliminary experimental study is also done to see the effectiveness of the proposed technique over classical control methods.

1. Introduction

Identification and control of flexible structures has received considerable attention in literature. Much of the research is motivated by the space industry, where large, lightly damped, flexible structures characterized by closely spaced modes and low natural frequencies are common. With the emergence of cheap microprocessors and smart materials like piezoelectric patches, electro-rheological fluids and magneto-rheological fluids, active vibration control is being used for automobile industry and manufacturing process vibration attenuation.

Very accurate models are required for active vibration control due to inherent small stability margins present for the non-collocated sensors and actuators. The un-modeled dynamics, component degradation, changing configuration and changing payloads can destabilize a fixed gain controller-based on nominal system

*Corresponding author. Tel.: +91 9888535359.
E-mail addresses: rajivsharma1972@yahoo.com (R. Kumar), singhsp@mech.iitd.ernet.in (S.P. Singh).

0022-460X/$ - see front matter © 2007 Elsevier Ltd. All rights reserved.
doi:10.1016/j.jsv.2007.06.028

model. Considering this, Tzes and Yurkovich [1,2] developed a time varying, non-parametric transfer function estimation scheme for flexible structure identification.

Recently, an intensive effort is being done to implement the adaptive control techniques to active vibration control of smart structures. In this direction, Zeng et al. [3] applied output feedback variable structure adaptive control to a flexible spacecraft. By using the neural network-based adaptive control strategy; Youn et al. [4] controlled the composite beam vibrations subjected to sudden de-lamination. Feedback controllers are suitable for random disturbances causing free vibrations. Shaw [5] used self-tuning regulators combined with minimum variance controller to control a spring mass system. Using classical positive position feedback control strategy, Rew et al. [6] suppressed multimodal vibrations of flexible structures. Model predictive control is an indispensable control technique in process control. By using the adaptive predictive control strategy, Bai et al. [7] suppressed rotor vibrations. More recently, Lim et al. [8] used adaptive bang–bang control for the vibration control of civil structures while seismic vibrations occur. Xiangzhu et al. [9] used ARMAX-based identification and pole placement-based controller for active vibration control of a smart beam.

Yang et al. [10] presented a vibration suppression scheme for an axially moving string under a spatiotemporally varying tension and an unknown boundary disturbance. The axially moving string system was divided into two spans, i.e. a controlled span and an uncontrolled span by a hydraulic touch roll actuator. They modeled the system as a hyperbolic partial differential equation describing the dynamics of the moving string. The actuator dynamics was derived using Hamilton principle. Lyapunov method was employed to design a robust adaptive boundary control law. Input shaping is an effective feed forward control design strategy. In this direction, Cutforth et al. [11] used adaptive input shaping control for controlling the vibrations in flexible structures. They explored the idea of adaptive input shaping which allows a fast input shaper to be used for providing robustness to parametric uncertainty. The adaptive input shaping method was capable of adaptation during maneuvers. Shape memory alloys (SMA) are an effective smart material in which the dimensions of the structure change when these are subjected to a change in temperature. A large strain rates can be easily attained. If the overall system comes under slow dynamics, these can be used effectively to control the system. Xu et al. [12] developed a shape memory alloy wall joint which can adaptively attenuate and control the vibration wave propagation in cylindrical shells. Since the parameters of a SMA joint can be tuned adaptively, the incident wave with different frequencies can be highly attenuated and controlled.

Kumar et al. [13] presented experimental adaptive identification and control of a smart structure featuring piezoceramic-based sensors/actuators. An inverted L-structure with surface-bonded piezoceramic sensors/actuators was used for analysis which is a partial representative of the *radial drilling machine* and *Selected Compliance Assembly Robot Arm* (SCARA). This structure is also extensively used in flexible spacecrafts. Multi-input multi-output (MIMO) linear quadratic regulator (LQR) was designed and implemented. It was assumed that the parameters of the smart structure were changing. Closed-loop (CL), time-domain identification of system parameters in auto-regressive moving average (ARMA) form, was proposed for the systems changing at slow rates. A thorough study was done to see the effect of updated system and controller parameters on system performance using adaptive control strategy.

Lin et al. [14] investigated vibration control of a smart beam using piezoelectric damping–modal actuators/sensors. Laminated composite beams with integrated sensors and actuators were analyzed. Emphasis in their study was given to the fiber orientation and effect of actuator location on the control system. An instantaneous, optimal CL control algorithm was used for the adaptive shape control of the dynamic response of the integrated laminated structure.

Kumar et al. [15] extended their previous work on inverted L structure. In this work, they observed that, to maintain stability, different set of feedback control gains should be applied for free and forced vibration attenuation. For forced vibrations, feedback controllers with certain optimum position of CL poles give maximum vibration reduction. By combining the feedback and feed forward controller (i.e. by using a hybrid controller), better transient performance can be obtained in case of forced vibrations. By adapting the controller (feed forward and feedback) parameters the CL system performance remained excellent for large variations in system parameters. Further, Kumar et al. [16] presented a comparative study of adaptive controllers based on minimum variance, pole placement and linear quadratic techniques. It was observed that

the controllers based on minimum variance are noise sensitive and actuator voltage changes sign after each sampling interval. Hence, this control strategy gives control signals which are detrimental to the life of piezoelectric actuators. Adaptive controller based on pole placement technique requires high control effort and gives poor performance at and near the nominal system. But, it was observed that the linear quadratic control-based adaptive controllers are noise tolerant and are free from the above-mentioned limitations.

Cables and strings also form a major component of practical structures and installations. Chen et al. [17] investigated adaptive vibration control for axially moving strings with a tensioner. The Lyapunov analysis was employed to design the controller. The proposed controller was capable of estimating the parameters online. The Lyapunov stability guarantees the convergence of the transverse vibration of the controlled span of the string as well as the estimation error of the unknown parameters to zero. Maganti et al. [18] presented a simple adaptive system for the rotational maneuver and vibration suppression of an orbiting spacecraft with flexible appendages. It was assumed that the system parameters were unknown and the truncated model of the spacecraft has finite but arbitrary dimensions. For the synthesis of control system, measured output error and the states of a third-order command generator were used.

Song et al. [19] investigated a nonlinear model-based adaptive suspension control system using Magneto-theological (MR) dampers. MR dampers have strong nonlinearities which can be modeled as mathematical functions. So, the model-based adaptive control algorithms become complicated. The objective of their study was to investigate the effect of MR model simplifications on the adaptive suspension performance. Numerical simulations were carried out to prove the efficiency of the proposed controller.

Recently, Kumar et al. [20] investigated in detail that the fixed controllers could become even unstable, with large changes in system parameters. Robust control and adaptive control design techniques were investigated in this work. Obviously, to obtain robust performance, it is desirable that the CL poles of the perturbed structure remain at pre-specified locations for a range of system parameters. For this, the controller designed based on pole placement method is quite useful. In their work, the controllers based on adaptive and robust pole placement method were implemented on smart structures. It was observed that, adaptive pole placement controllers were noise tolerant, but required high actuator voltages to maintain stability. However, robust pole placement controllers require comparatively small amplitude of control voltage to maintain stability, but are noise sensitive.

Classical adaptive controllers based on adaptive parameters estimation *work efficiently if the system dynamics is slow and the system parameters are changing slowly with time*. However, in vibration control, where system dynamics is quite fast and the parameters can change abruptly, the efficiency of these controllers degrades. *Either the CL performance is poor or the transient response is unacceptable*. The system parameters in the above cases change quickly as relative configuration of various arms changes. System parameters are also affected as payloads are changed. For these situations, multivariable adaptive controllers using computationally intensive methods of parameter estimation cannot be implemented with windows-based operating systems. Fortunately, for these cases, the mode of change of system parameters is known a priori (i.e. either by change in relative configuration or by change in payload).

System classification technique based on unsupervised and supervised learning is quite suitable for these situations. *Based on the prior knowledge of the mode of change of system, the system parameters, control gains and observer gains are calculated offline for various possible cases*. Using unsupervised learning techniques the various systems can be classified into discrete number of classes. Using Learning Vector Quantization (LVQ) neural networks, these systems can be classified into different classes using *first few natural frequencies as separating criteria*. In the present study, these systems are classified based on the first two natural frequencies. These natural frequencies can be found from spectrum analyzer in real time. Based on these frequencies, the *class of the system parameters*, *control gains and observer gains* is found using trained LVQ neural networks. By applying the system matrices, control gains and observer gains, *identified* for that particular class, system performance can be improved drastically as compared to non-adaptive control as well as classical adaptive control techniques. The experimental results indicate that a *better transition period performance* can be obtained with the proposed technique as compared to other adaptive control methods. As seen in Ref. [16], Linear Quadratic Control strategy gives best results, hence adopted in the present work.

2. Mathematical modeling of smart structures

Schematic diagram of the proposed inverted L structure is shown in Fig. 1. The structure is mounted with two piezoceramics patches bonded on its surface acting as actuators and other two piezoceramic patches bonded on surface acting as sensors.

2.1. Finite element modeling

Lagrange's equations of motion for linear systems is

$$\sum_{s=1}^{n}\left[m_{js}\ddot{y}_s(t)+c_{js}\dot{y}_s(t)+k_{js}y_s(t)\right]=Q_j(t), \qquad j=1,2,\ldots,n, \tag{1}$$

where $y(t)$ is the physical displacement, $\dot{y}(t)$ is physical velocity and $\ddot{y}(t)$ is the physical acceleration at time instant 't' for the particular degree of freedom. Also m, c and k are the elements of mass, damping and stiffness respectively. Relation (1) represents a set of n simultaneous second-order ordinary differential equations in generalized coordinates. By using this relation, the infinite degree of freedom distributed system is approximated by an n-degree of freedom system. This relation can be written in matrix form as [21,22]

$$\mathbf{M}\ddot{\mathbf{y}}(t)+\mathbf{C}\dot{\mathbf{y}}(t)+\mathbf{K}\mathbf{y}(t)=\mathbf{Q}(t), \tag{2}$$

where **M**, **C** and **K** are the global mass, damping and stiffness matrices, respectively, and **Q** (t) is the vector of physical applied forces at various degrees of freedom at time t. The column vector **y**(t) is the nodal (also called physical) displacements at time t. *The inverted L structure can be assumed to be made by joining two beams perpendicular to each other.* Table 1 and Fig. 1 show the mechanical properties and geometrical parameters of the structural system. The structure is divided into 12 elements (i.e. two-dimensional beam elements) with 3 degrees-of-freedom at each node. Two of these are the deflections in x and y-direction and the third one is the rotation about z-direction. One-dimensional beam elements have only 2 degrees of freedom at each node and hence unsuitable for modeling the L structure. Global mass and stiffness matrices are found by joining the elemental matrices. The damping ratios are obtained by modal analysis. Using the Matrix Iteration method [21], the eigenvalue problem can be solved to give the natural frequencies and mode shapes for various tip loads ranging from 2 to 20 g. Using the coupled control technique [22], the system can be written in state-space form [23] and is discussed in next subsection.

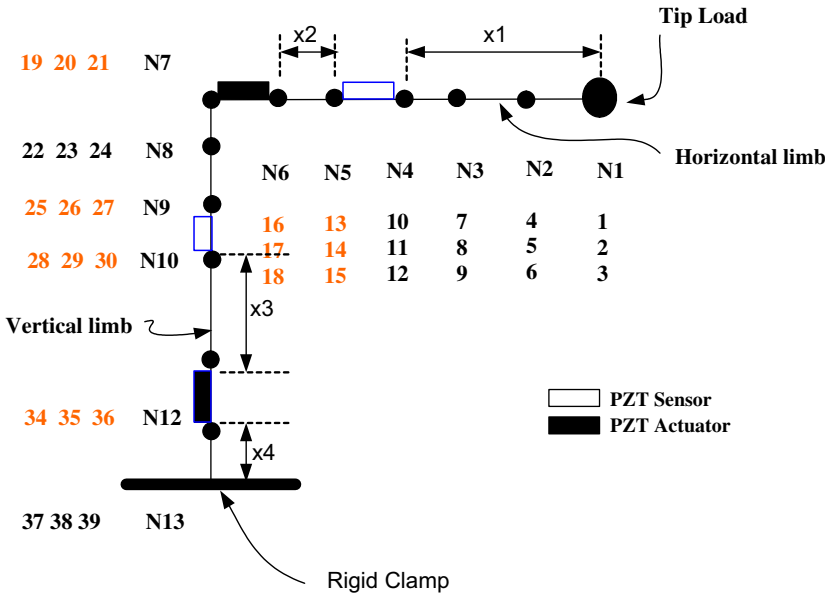

Fig. 1. Discretization of inverted L structure.

Table 1
Geometrical and mechanical properties

Property	Material		
	Steel structure		PZT patches
Maximum length of horizontal limb (mm)	100		–
Maximum length of vertical limb (mm)	100		–
Thickness (mm)	1		1
Length of PZT patch (mm)	–		20
Width (mm)	10		10
Young's Modulus (MPa)	210		64
Density (kg/m^3)	7800		7650
x_1 (mm)		50	
x_2 (mm)		10	
x_3 (mm)		20	
x_4 (mm)		5	

2.2. State-space modeling

For the system having 'r' modes, the system dynamics can be written in matrix state space form as given below

$$\begin{aligned}\dot{\zeta}(t) &= \alpha\zeta(t) + \boldsymbol{\beta}\upsilon(t),\\ \boldsymbol{\lambda}(t) &= \boldsymbol{\gamma}\zeta(t),\end{aligned} \tag{3}$$

where the modal state vector $\dot{\zeta}(t)$ by

$$\zeta(t) = [\zeta_1(t) \quad \zeta_2(t) \quad \zeta_3(t) \quad \zeta_4(t) \quad \zeta_{2r-1}(t) \quad \zeta_{2r}(t)]^{\mathrm{T}}$$

and $\boldsymbol{\alpha}$, $\boldsymbol{\beta}$ and $\boldsymbol{\gamma}$ are called system matrices and can be obtained in the modal domain as described by Meirovitch [22].

State coupling matrix

$$\boldsymbol{\alpha} = \begin{bmatrix} 0 & 1 & 0 & 0 & \dots & \dots & 0 & 0 \\ -\omega_1^2 & -2\varsigma_1\omega_1 & 0 & 0 & \dots & \dots & 0 & 0 \\ 0 & 0 & 0 & 1 & \dots & \dots & 0 & 0 \\ 0 & 0 & -\omega_2^2 & -2\varsigma_2\omega_2 & \dots & \dots & 0 & 0 \\ \vdots & \vdots & \vdots & \vdots & \ddots & \ddots & \vdots & \vdots \\ \vdots & \vdots & \vdots & \vdots & \ddots & \ddots & \vdots & \vdots \\ 0 & 0 & 0 & 0 & \dots & \dots & 0 & 1 \\ 0 & 0 & 0 & 0 & \dots & \dots & -\omega_r^2 & -2\varsigma_r\omega_r \end{bmatrix}, \tag{4a}$$

Input coupling matrix

$$\boldsymbol{\beta} = \begin{bmatrix} 0 & 0 & 0 & 0 & \dots & 0 \\ {}^{(1)}\Phi_1 & {}^{(1)}\Phi_2 & {}^{(1)}\Phi_3 & {}^{(1)}\Phi_4 & \dots & {}^{(1)}\Phi_a \\ 0 & 0 & 0 & 0 & \dots & 0 \\ {}^{(2)}\Phi_1 & {}^{(2)}\Phi_2 & {}^{(2)}\Phi_3 & {}^{(2)}\Phi_4 & \dots & {}^{(2)}\Phi_a \\ \vdots & \vdots & \vdots & \vdots & \ddots & \vdots \\ 0 & 0 & 0 & 0 & \dots & 0 \\ {}^{(r)}\Phi_1 & {}^{(r)}\Phi_2 & {}^{(r)}\Phi_3 & {}^{(r)}\Phi_4 & \dots & {}^{(r)}\Phi_a \end{bmatrix}, \tag{4b}$$

Output coupling matrix

$$\gamma = \begin{bmatrix} {}^{(1)}\Phi_1 & 0 & {}^{(2)}\Phi_1 & 0 & \dots & {}^{(r)}\Phi_1 & 0 \\ {}^{(1)}\Phi_2 & 0 & {}^{(2)}\Phi_2 & 0 & \dots & {}^{(r)}\Phi_2 & 0 \\ {}^{(1)}\Phi_3 & 0 & {}^{(2)}\Phi_3 & 0 & \dots & {}^{(r)}\Phi_3 & 0 \\ {}^{(1)}\Phi_4 & 0 & {}^{(2)}\Phi_4 & 0 & \dots & {}^{(r)}\Phi_4 & 0 \\ \vdots & \vdots & \vdots & \vdots & \ddots & \vdots & \vdots \\ \vdots & \vdots & \vdots & \vdots & \ddots & \vdots & \vdots \\ {}^{(1)}\Phi_s & 0 & {}^{(2)}\Phi_s & 0 & \dots & {}^{(r)}\Phi_s & 0 \end{bmatrix}, \tag{4c}$$

where ω_r is the natural frequency and ς_r is the damping ratio at the rth mode, ${}^{(r)}\Phi_a$ is the mode shape difference at the two ends of the piezoelectric patch at actuator 'a' and ${}^{(r)}\Phi_s$ is the mode shape difference at the two ends of the piezoelectric patch at sensor 's'. This continuous time system is converted into discrete time system using bilinear transformations at a desired sampling time and we then get the following form [23]:

$$\begin{aligned} \xi(k+1) &= \mathscr{F}\xi(k) + \mathscr{G}\upsilon(k), \\ \chi(k) &= \mathscr{H}\xi(k). \end{aligned} \tag{5}$$

2.3. Piezoelectric sensing and actuation

When a piezoelectric patch, attached to the distributed structure, is subjected to a change in slope at its two edges, electric charge is developed inside the system. This charge developed in the PZT patch mounted on steel structure is given by Buttler and Rao [24]

$$\delta(t) = \frac{1}{2}(t_s + t_p)(d_{31} + \upsilon_p d_{32})\frac{E_p}{1-\upsilon_p^2} b(\theta_2(t) - \theta_1(t)), \tag{6}$$

where $\theta_2(t)$ and $\theta_1(t)$ are, respectively, the slopes of end 1 and end 2 of the PZT patch at the instant of time 't'. The thickness of steel and PZT patch are denoted by t_s and t_p, respectively. The dielectric constants of the PZT material are denoted by d_{31} and d_{32}. The breadth of the steel beam and piezoelectric patch is denoted by b. The value of Young's modulus of elasticity and Poisson's ratio for the PZT material are denoted by E_p and υ_p, respectively. Similarly the value of Young's modulus of elasticity and Poison's ratio for the steel beam are denoted by E_s and υ_s, respectively. The values of these parameters are given in Tables 1 and 2. The voltage developed due to this charge is given by Buttler and Rao [24]

$$V(t) = \frac{\delta(t)t_p}{\varepsilon_p A_p}, \tag{7}$$

where A_p is the area of PZT patch and ε_p is the permittivity of the PZT material. Since all values except $\theta_1(t)$ and $\theta_2(t)$ are constant in Eqs. (6) and (7), Eq. (7) may be written as $V(t) = \Gamma(\theta_2(t) - \theta_1(t))$. Γ is the conversion coefficient.

When a voltage 'V' volt is applied across the piezoelectric patch, the bending moment 'M_f' of opposite sense is produced at both the edges. Value of this bending moment is given by Baz and Poh [25] as

$$M_f = \left[\frac{d_{31} b E_p\left(E_s t_p t_s + E_s t_b^2\right)}{2\left(E_p t_p + E_s t_s\right)}\right] V. \tag{8}$$

Since all the parameters except V are constant in Eq. (8), the subsequent relation may be written as M_f (N m) $= \Psi V$ (V). Ψ is the conversion coefficient.

Table 2
Electrical properties of PZT

Property	Symbol	Value
Piezoelectric charge constant ($m V^{-1}$)	d_{31}	171×10^{-12}
Piezoelectric charge constant ($m V^{-1}$)	d_{32}	171×10^{-12}
Poisson's ratio	υ_p	0.28
Permittivity ($F m^{-1}$)	ε	106×10^{-12}

2.4. Difference equation (DE) and matrix fraction description (MFD) modeling

State-space form of system parameters is quite suitable for controller design purposes. But, it is difficult to identify the system parameters in this form. Unfortunately, the adaptive controller cannot be designed easily for this form. However, using difference equation form, identification task becomes quite easy. Hence, some transformations are needed to convert the system from state-space form to difference equation form and vice versa in a unique way. In case, the finite element techniques are not to be used, system identification techniques can also be applied for mathematical modeling. For that, these transformations are quite helpful.

Defining the transformation matrix $\mathscr{T}$ by Guidorzi [26,27]

$$\mathscr{T}^{\mathrm{T}} = \begin{bmatrix} \mathscr{H}_1 & \mathscr{F}^{\mathrm{T}}\mathscr{H}_1 & \mathscr{H}_2 & \mathscr{F}^{\mathrm{T}}\mathscr{H}_2 \end{bmatrix}. \tag{9}$$

Using the transformation matrix $\mathscr{T}$, we obtain the new state vector

$$\psi = \mathscr{T}\xi. \tag{10}$$

Eq. (5) is transformed to unique canonical form, using transformation matrix $\mathscr{T}$, by the following relation:

$$\mathscr{T}\xi(k+1) = \mathscr{T}F\mathscr{T}^{-1}\mathscr{T}\xi(k) + \mathscr{T}\mathscr{G}\upsilon(k) \text{ and } {}_{\mathscr{Y}}(k) = \mathscr{H}\mathscr{T}^{-1}\mathscr{T}\xi(k) \tag{11}$$

Substituting

$$\mathscr{T}\xi(k+1) = \psi(k+1), \quad \mathscr{T}\mathscr{F}\mathscr{T}^{-1} = \mathscr{A}, \quad \mathscr{T}\mathscr{G} = \mathscr{B} \quad \text{and} \quad \mathscr{H}\mathscr{T}^{-1} = \mathscr{C} \tag{12}$$

The following relations are obtained:

$$\begin{aligned} \psi(k+1) &= \mathscr{A}\psi(k) + \mathscr{B}u(k) \\ {}_{\mathscr{Y}}(k) &= \mathscr{C}\psi(k) \end{aligned} \tag{13}$$

The system as described in the above Eq. (13) is unique. It can be now transformed into difference equation form in a unique fashion. As discussed earlier that for system identification, Auto Regressive Moving Average (ARMA) difference equations are more useful. The above state-space form can be converted into the difference equations form, given below, using the technique discussed in Appendix and in Refs. [26,27]:

$$\mathbf{P}_0\mathbf{y}(t) + \mathbf{P}_1\mathbf{y}(t-1) + \mathbf{P}_2 y(t-2) + \cdots + \mathbf{P}_\mathbf{r}\mathbf{y}(t-r) = \mathbf{Q}_1\mathbf{u}(t-1) + \mathbf{Q}_2\mathbf{u}(t-2) + \cdots + \mathbf{Q}_\mathbf{r}\mathbf{u}(t-r), \tag{14}$$

where $\mathbf{P}$'s and $\mathbf{Q}$'s are coefficient matrices of the difference equation. This is a rth-order (by considering first r-modes), l-input, m-output, multivariable system, represented by input–output difference equation model with $\mathbf{u}(t) = [u_1(t)\, u_2(t) \ldots u_l(t)]^{\mathrm{T}}$ and $\mathbf{y}(t) = [y_1(t)\, y_2(t) \ldots y_m(t)]^{\mathrm{T}}$. This difference equation represents the same dynamics as Eq. (13). The system can then be written in MFD form as [26,27]

$$\mathbf{W} = \mathbf{A}^{-1}\mathbf{B}, \tag{15}$$

where $\mathbf{A}$ and $\mathbf{B}$ are polynomial matrices. For a 2-input, 2-output, second-order system, used in the present work, results in Appendix can be used.

3. Linear quadratic gaussian (LQG) controller

LQG controller, which is a combination of LQR and Kalman Filter, has been implemented for each state of the system. The important features of the controller are discussed in the following sections.

3.1. Modeling the noise characteristics

To estimate the states of the system accurately, noise characteristics must be known. Two types of noises are considered viz. measurement noise and process noise [23]. The measurement and process errors have been considered with zero mean. The noise-free part of the signal is obtained by repeating the experiment several times for an input sequence and taking the average of that output sequence. In the present case, $N = 1024$ points are taken to construct one full waveform. The measurement noise vector $\mathbf{v}(k)$ is estimated by subtracting the system output from the average output for a particular input sequence. Similarly for process noise vector $\mathbf{w}(k)$ is generated.

3.2. State feedback LQG controller

LQR with Kalman filter has proved to be an excellent robust control system design methodology. Relation (5) represents the system to be controlled in state space form. Due to the presence of 'Measurement Noise' and 'Process Noise' the system state and output equations of the stochastic system have the following form [23]:

$$\begin{aligned} \psi(k+1) &= \mathscr{A}\psi(k) + \mathscr{B}u(k) + \mathbf{w}(k) \\ \mathscr{y}(k) &= \mathscr{C}\psi(k) + \mathbf{v}(k) \end{aligned} \tag{16}$$

where $\mathbf{v}(k)$ is the measurement noise vector and $\mathbf{w}(k)$ is the process noise vector. The corresponding difference equation model is written as follows:

$$\begin{aligned} &\mathbf{P}_0\mathbf{y}(t) + \mathbf{P}_1\mathbf{y}(t-1) + \mathbf{P}_2\mathbf{y}(t-2) + \cdots + \mathbf{P}_\mathbf{r}\mathbf{y}(t-r) + \mathbf{S}_0\mathbf{y}(t) + \mathbf{S}_1\mathbf{y}(t-1) + \mathbf{S}_2\mathbf{y}(t-2) + \ldots + \mathbf{S}_\mathbf{s} \\ &\mathbf{y}(t-s) = \mathbf{Q}_1\mathbf{u}(t-1) + \mathbf{Q}_2\mathbf{u}(t-2) + \cdots + \mathbf{Q}_\mathbf{r}\mathbf{u}(t-r), \end{aligned} \tag{17}$$

where $\mathbf{S}$'s are the coefficient matrices. These matrices correspond to a noise model of order s. Eq. (17) can be converted to equivalent MFD form represented by following relation:

$$\mathbf{W} = \mathbf{A}^{-1}\mathbf{B} + \mathbf{A}^{-1}\mathbf{C}, \tag{18}$$

where $\mathbf{C}$ represents a polynomial matrix in MFD form constructed from noise covariances using Appendix or Refs. [26,27].

In state space form, to calculate the control signal, states of the system are needed. Using the inputs $\mathscr{u}(k)$ and outputs $\mathscr{y}(k)$ the future state vector $\boldsymbol{\psi}(k+1)$ can be estimated accurately by using Kalman Filter.

Using the gain matrix $\mathbf{K}$, control inputs are calculated by the following equation:

$$\mathscr{u}(k) = -\mathbf{K}\boldsymbol{\psi}(k). \tag{19}$$

The system matrices $\mathscr{A}$ and $\mathscr{B}$ and the weighing matrix $\mathscr{R}$ and $\mathscr{Q}$ are used to calculate the gain matrix $\mathbf{K}$. The relative amplitude of the elements of these matrices determines the amplitude of the control signal vector $\mathscr{u}(k)$.

3.3. Output feedback LQG controller

Polynomial-based controller design techniques are best suitable for adaptive control. In this approach, spectral factorization algorithms are often used [28]. To implement the LQG controller two different strategies are implemented, implicit and explicit. In implicit form, the controller parameters are directly adapted using input–output data. In explicit form, first of all system parameters are adapted and after that controller parameters are identified or updated. The detailed method to implement this controller is explained in Ref. [29]. Explicit LQG adaptive controllers are easy to implement as compared to implicit LQG controller. However, the computational burden of the former is slightly more than the later.

The algorithm to implement this controller is discussed below:

(1) Chose the cost function weighing polynomial matrices $\boldsymbol{\varphi}_1$ and $\boldsymbol{\varphi}_2$.. Here $\boldsymbol{\varphi}_1$ is the output (error) weighing matrix; $\boldsymbol{\varphi}_2$ is the control weighing matrix appropriate for matrix transfer function.
(2) Estimate the coefficients $\mathbf{P}_0$, $\mathbf{P}_1$, …, $\mathbf{P}_r$, $\mathbf{S}_0$, $\mathbf{S}_1$, …, $\mathbf{S}_s$ and $\mathbf{Q}_1$, $\mathbf{Q}_2$, …, $\mathbf{Q}_r$ of difference equation in matrix form using least-squares method along with covariances ψ_1 and ψ_2.

(3) Find **A**, **B** and **C** in MFD form using Appendix and Refs. [26,27]
(4) Calculate the stable spectral factor **D** using

$$\bar{\mathbf{C}}\boldsymbol{\varphi}_1\mathbf{C} + \bar{\mathbf{A}}\boldsymbol{\varphi}_2\mathbf{A} = \overline{\mathbf{D}}\mathbf{D}, \tag{20}$$

where scalar $\bar{C} = 1 + C_1 z^1 + C_2 z^2 + \cdots$, if scalar $C = 1 + C_1 z^{-1} + C_2 z^{-2} + \cdots$.
Similarly scalar $\bar{A} = 1 + A_1 z^1 + A_2 z^2 + \cdots$, if scalar $A = 1 + A_1 z^{-1} + A_2 z^{-2} + \cdots$.
(5) Calculate the stable spectral $\mathbf{D}_1$ using

$$\bar{\mathbf{B}}\boldsymbol{\psi}_1\mathbf{B} + \bar{\mathbf{A}}\boldsymbol{\psi}_2\mathbf{A} = \bar{\mathbf{D}}_1\mathbf{D}_1, \tag{21}$$

where scalar $\bar{B} = 1 + B_1 z^1 + B_2 z^2 + \cdots$, if scalar $B = 1 + B_1 z^{-1} + B_2 z^{-2} + \cdots$.
Similarly scalar $\bar{A} = 1 + A_1 z^1 + A_2 z^2 + \cdots$, if scalar $A = 1 + A_1 z^{-1} + A_2 z^{-2} + \cdots$.
(6) Calculate

$$\mathbf{D}_1\mathbf{D}. \tag{22}$$

(7) Calculate the controller $\mathbf{G_0/H_0}$ **in** MFD form using the equation

$$\mathbf{AH}_0 + \mathbf{BG}_0 = \mathbf{D}_1\mathbf{D}. \tag{23}$$

(8) Convert the controller in polynomial difference equation form using Appendix and Refs. [26,27]

4. Adaptive control using neural networks

4.1. System classification using unsupervised learning

The system matrix $(\mathscr{A}, \mathscr{B}, \mathscr{C})$ depends upon system's natural frequencies and mode shapes. As the payload changes from zero to a maximum specified value considered for the system, the system's natural frequencies are changed. So there is direct relationship between tip payload and system matrices. For each payload the system has distinct natural frequencies. Also with the change in relative configuration of the respective arms of the inverted L structure, system's natural frequencies are changed. The first three natural frequencies of the flexible structure, for various combination of vertical limb length, horizontal limb length and tip load are calculated. In the present study, length of the vertical limb is varied from 74 to 100 mm with 74, 85, 95 and 100 as intermediate steps. Length of horizontal limb varies from 84 to 100 mm with 84, 90, 95 and 100 as intermediate steps. The tip load varies from 2 to 20 g with step of 2 g. Total of 160 combinations are formed ($4 \times 4 \times 10$). The frequencies and mode shapes are calculated using FEM techniques for all the 160 systems. It has been observed that for all the possible combinations of vertical limb length, horizontal limb length and payload, first three natural frequencies are never equal. At the most two frequencies match. The third natural frequency varies considerably. Table 3 shows important sets with certain combinations of relative lengths and payloads, which have matching frequencies. To check the efficiency of the finite element model the natural frequencies of the structure with various combinations of length and payload are measured experimentally (Table 4). This data shows the good match between theoretical and experimental results. Observing precisely, it is noted that there is a unique combination of three frequencies for a particular class. Not all the three frequencies are equal simultaneously. At the most two frequencies can be similar, but the third frequency differs. So, all the systems can be classified distinctly based on these first three natural frequencies but it is not desirable due to following reasons:

(1) A large number of classes are generated, which is not desirable from the point of view of system classification.
(2) According to sampling theorem, to distinguish the various frequencies, the sampling frequency of the system should be at least twice the highest frequency content. So, the high value sampling frequency is

Table 3
First three natural frequencies at different configurations and tip loads

Length of horizontal limb (cm)	Length of horizontal limb (cm)	Payload (g)	Natural frequency (Hz)			Case number
			I	II	III	
100	100	2	29.14	74.24	362.04	1
95	95	2	29.11	74.91	354.11	52
74	95	4	28.28	79.78	329.62	75
100	90	2	28.77	75.30	369.04	82
95	90	2	30.42	78.51	383.60	92
74	90	4	29.90	82.31	363.41	115
95	84	2	29.51	76.39	395.90	133
74	84	6	28.29	79.02	399.64	157

Table 4
Table showing experimentally determined first three natural frequencies at different configurations and tip loads

Tip load (g)	Natural frequency (Hz)					
	First		Second		Third	
	Theoretical	Experimental	Theoretical	Experimental	Theoretical	Experimental
2	29.14	29	74.24	71	362.04	356
10	16.70	18	47.61	47	266.85	261

required. This means more control calculations have to be performed in a small period of time (i.e. in a sampling period). This needs computational machinery of very high power.

(3) Practically, only the first two modes are primarily excited in the present case of inverted L structure.

So, the next simplification is to neglect the third natural frequency. With this approach, all the 160 systems with different tip loads and relative configurations can be classified into a small number of classes (Fig. 2). Taking the certain length of the '*on-line*' data in time domain and using the spectral analysis techniques, the first two natural frequencies can easily be estimated. The system parameters are directly related with the natural frequencies, mode shapes and damping ratios (Eq. (4)).The first two frequencies are sufficient for the classification of different systems. This is due to the fact that the mode shapes and the damping ratios are not changed much for a particular geometry of structure. Fig. 3 shows the modal parameters as a function of payload or tip load. Frequencies are changing with a much higher order as compared to mode shape change at actuator as well as sensor position. Now, according to relation (4), the system matrices are much more dependent on system's frequencies. Flowchart as shown in Fig. 4 is used to classify the different systems into a small number of classes. First of all, the total number of systems is divided into a certain number of classes N. The weighing matrices $\mathscr{Q}$ and $\mathscr{R}$ are given a certain initial value. The neural networks working on unsupervised learning theory are used to classify the total data into N number of classes [31]. Then a competitive neural network is created. The optimum values of the frequencies corresponding to each class are calculated in such a manner that the sum of the squares of the difference between the frequencies corresponding to each element of that class and the optimum frequency values is minimum. Now these optimum frequencies are used to construct the system matrices $\mathscr{A}$, $\mathscr{B}$ and $\mathscr{C}$ (by using relation (4)). Afterwards, a LQR is designed by solving the Ricatti equation resulting in a gain matrix $\mathbf{K}$. Then, the CL stability of all the systems lying in a particular class is ensured by connecting the gain matrix $\mathbf{K}$ in feedback loop. This procedure is used for all the number of classes N. If the CL stability is not assured for even a single element of each class, the iteration loop is started by increasing the total number of classes from N to $N+1$. This loop continues till the CL stability of each system is assured. Total numbers of 32 classes (Fig. 5) are obtained at the end, covering all the 160 systems.

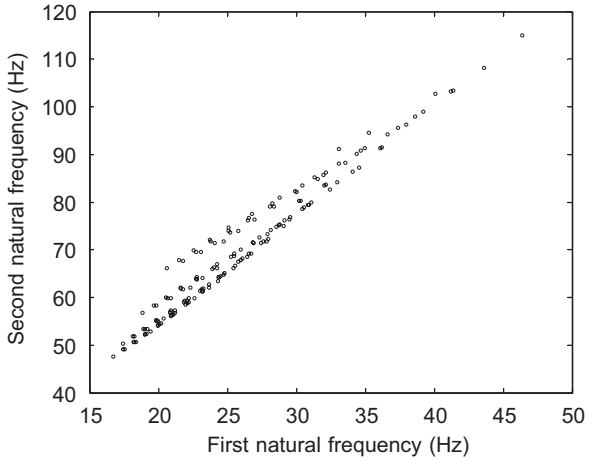

Fig. 2. System classification based on first two natural frequencies.

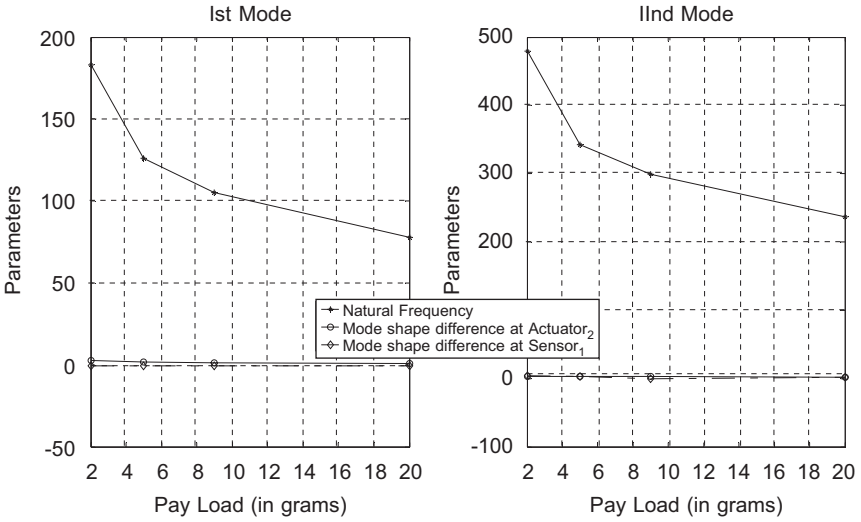

Fig. 3. Modal parameters as a function of payload.

The next step is to design the LQRs for each class, so that a uniform CL performance is maintained. This can be done by forcing the poles of the CL system in a specified region. For each class, the gain matrix **K** is calculated repeatedly by increasing the value of the weighing matrix $\mathscr{R}$ until all the CL poles lie in a certain specified stable region for all the N classes. Similar to the controller gain matrix, Kalman filter gain matrix is calculated offline for each class. These parameters are tabulated against the system's natural frequencies.

4.2. System classification based on supervised learning

By identifying system parameters offline for all possible configurations and using vector Quantization techniques, it is possible to categorize the system matrices based on natural frequencies. This gives accurate identification of system parameters. As LVQ networks are trained offline, computational burden is reduced. Hence this technique is suitable for online implementation. LVQ neural networks can easily classify the system parameters based on natural frequencies. The neural networks are trained for all the different set of classes based on first two natural frequencies. Only, offline computations are required for training of the neural

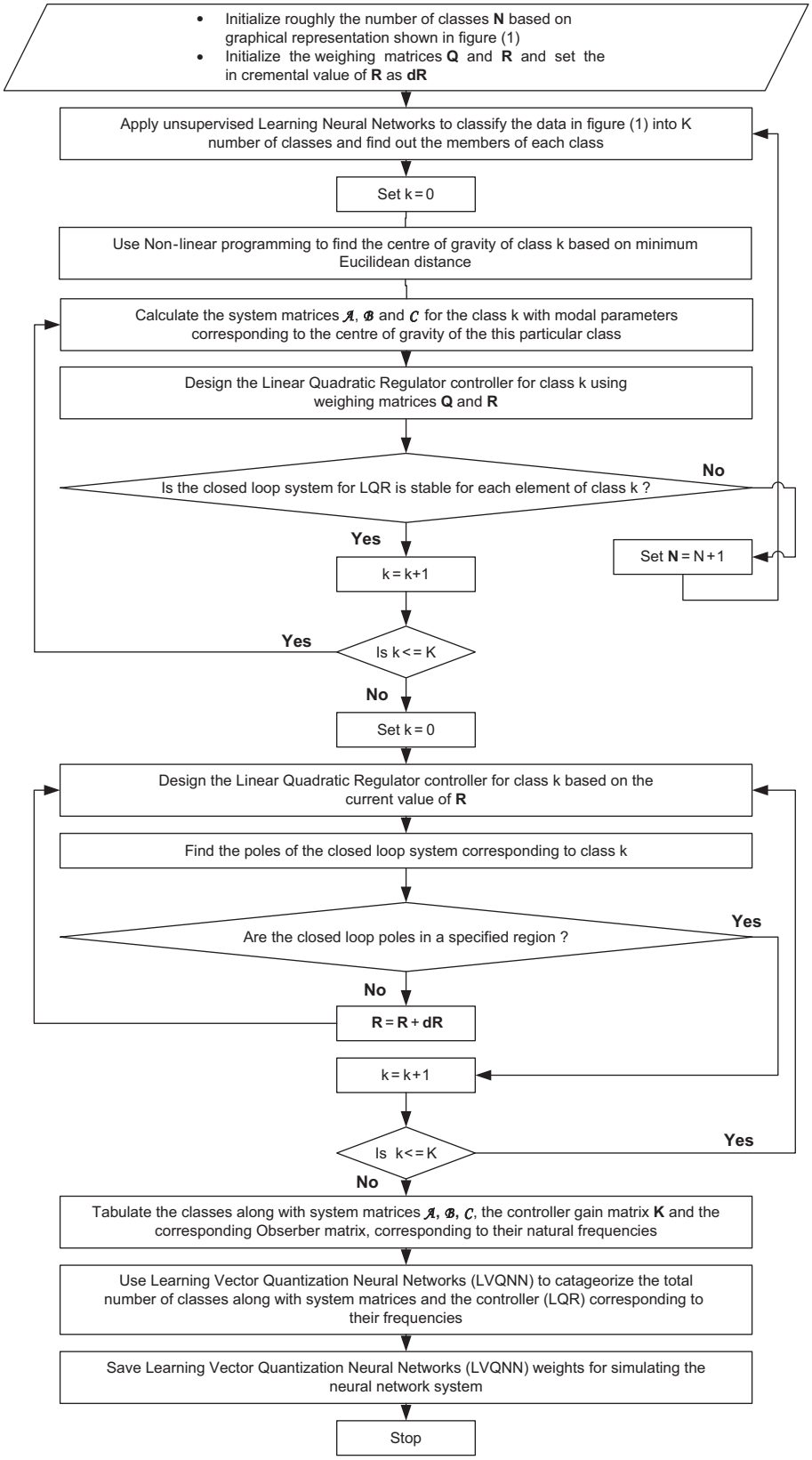

Fig. 4. Flow chart for system classification.

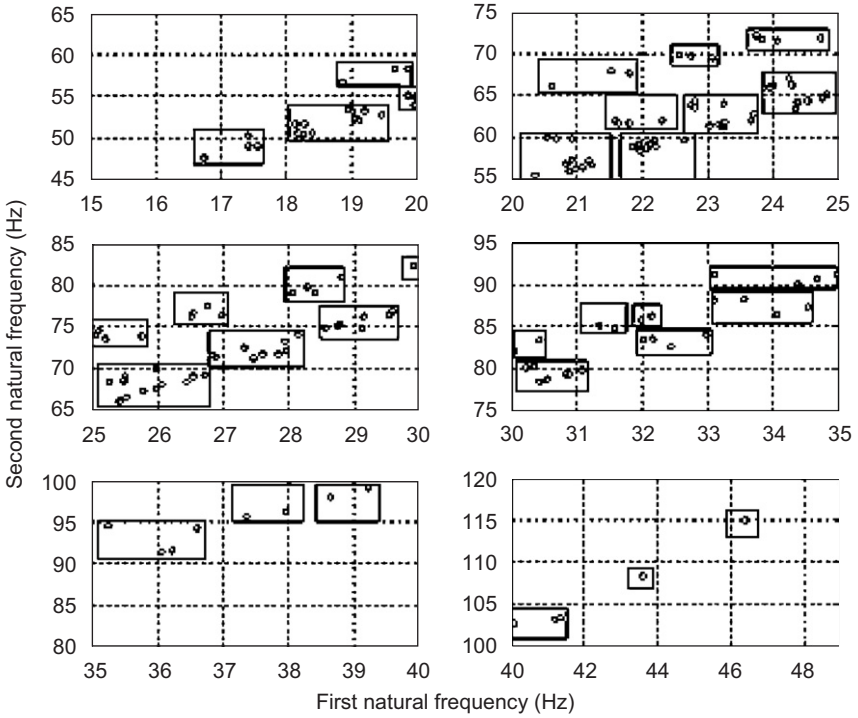

Fig. 5. Final system classification based on first two natural frequencies using the flow chart shown in Fig. 4.

networks. These trained weights can now be used online to identify a particular class of the system with certain system matrices, controller gains and observer gains. One thing worth mentioning is that an excitation signal of small amplitude and containing frequencies from 0 to 200 Hz is continuously applied to the structure during the identification phase for proper excitation of first two modes. Using the MATLAB toolbox [32], neural network is trained and the weights of the LVQ Neural Networks are saved for online use during actual experiment.

5. Experimental setup and procedure

The experimental apparatus for vibration control of smart structures is presented in Fig. 6. The signals from the PZT patches are fed to the data acquition card. The Analog-to-Digital (A/D) conversion and Digital-to-Analog (D/A) conversion one done through the data acquition card PXI-6062E of National Instruments, having 12 bit resolution for the A/D and D/A conversions. The applied control voltage varies from -220 to $+220$ V. High voltage amplifier was used to step up the voltage in this range, from -10 to $+10$ V supplied by the computer. A low pass filter is applied in the sensing process to avoid interference of higher modes. The Graphical Programming software Lab View is used for experimental implementation [33]. Real Time engine PXI-8187RT using Lab View RT is used to bear the computational burden of adaptive linear quadratic Gaussian control discussed in Section 3.3. An excitation signal with lower amplitudes, i.e. from -20 to $+20$ V, is applied during the identification phase to excite all the modes for accurate CL identification.

5.1. Design of excitation signal

For an accurate identification, any arbitrary signal may not be suitable. The input data supplied to the system for system identification should be informative [34]. Both for open loop (OL) and CL operations, 'informative' means that the input should be persistently exciting of a certain order, i.e. that it contains

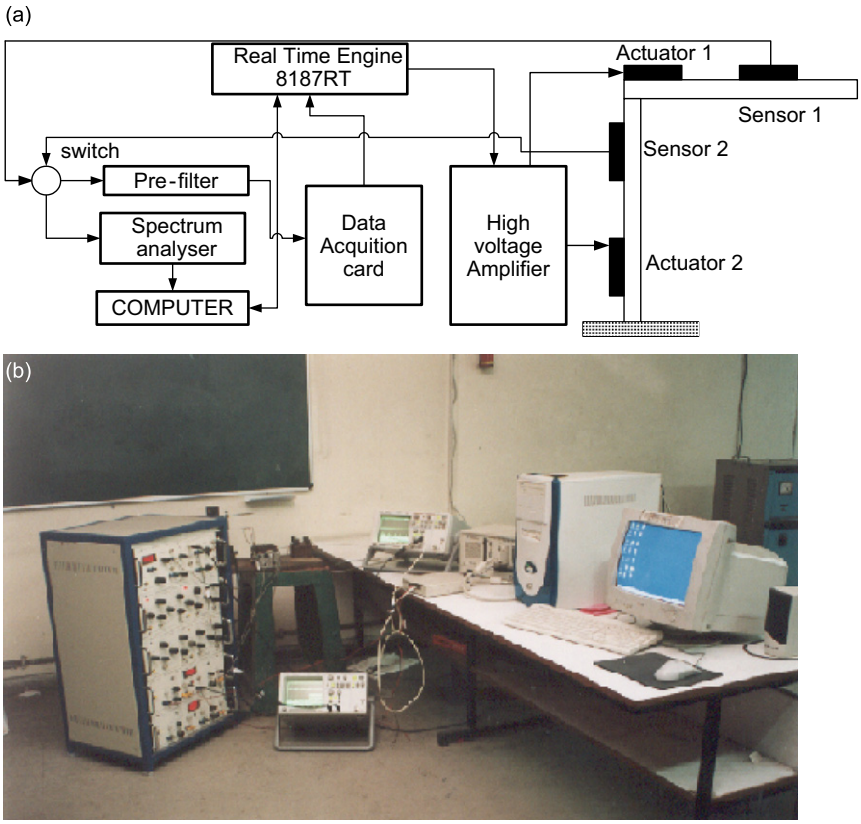

Fig. 6. (a) Schematic of experimental setup. (b) Photograph of the experimental setup.

sufficiently many distinct frequencies. For the identification of linear systems, there are three basic requirements that govern the choices:

(a) The asymptotic properties of the estimate (bias and variance) depend only on the input spectrum and not the actual waveform of the input.
(b) The input must have limited amplitude.
(c) Periodic inputs may have certain advantages.

Based on several factors, the classification of the input signal can be done into various categories, viz. Filtered Gaussian White Noise, Random Binary Signal, Pseudo-Random Binary Signal, MultiSines and Chirp Signals or Swept Sinusoids. In the present case, to excite the system in CL, the multisine wave with minimum crest factor [34] and magnitude of the excitation signal near 20 V was used.

5.2. *Combined identification and control algorithm*

In this section the system parameters are estimated based on the newly available data. Then the system matrices and controller are selected and are used for the control of new system to obtain the better performance of the control system. Fig. 7 shows the algorithm for online identification and adaptive vibration control. In the present case, to check the validity of the proposed technique, first two natural frequencies were used to classify the system corresponding to tip loads 2–20 g, for vertical and horizontal limb length of 100 mm. By using trained LVQ neural network whose weights are saved in a file, any of the 32 classes can be identified and are used for experimental validation of this technique. The power spectral density of the data from either sensor 1 or sensor 2 are calculated. The natural frequencies of the system are then obtained.

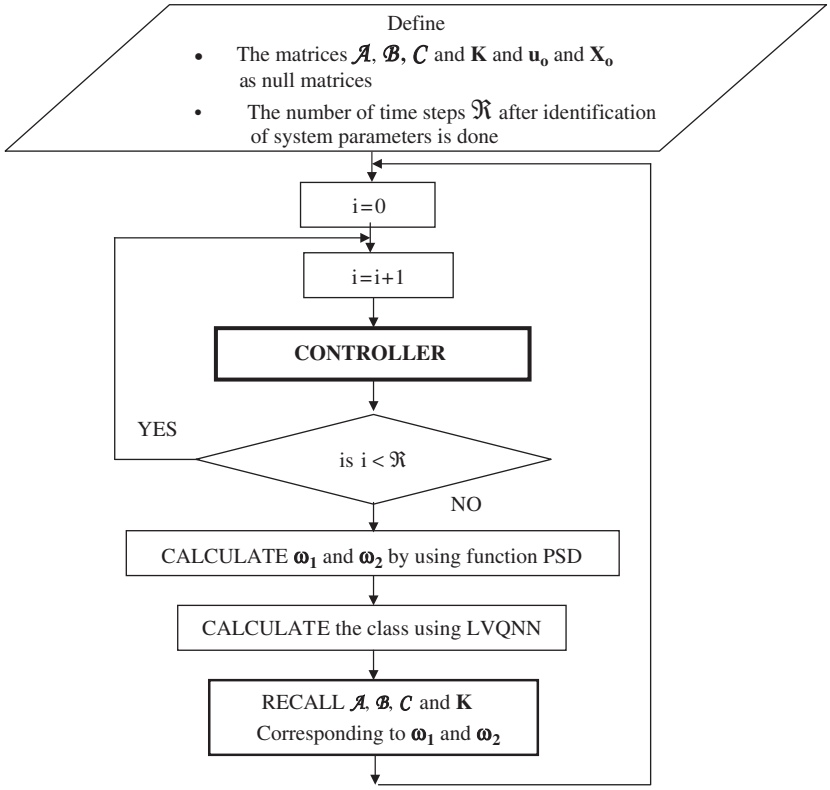

Fig. 7. Algorithm for Real-Time identification and Adaptive vibration control.

These natural frequencies are fed as input to the Learning Vector Quantization Neural Networks (LVQNN). A LVQ neural network has a first competitive layer and a second linear layer. First two natural frequencies are the inputs to the network. The competitive layer contains 32 neurons (equal to the number of classes in which data are to be clustered). The output of the LVQNN will be the identified class number. As already mentioned, Matlab toolbox is used to create, train and simulate the network (with 'newlvq', 'trainlvq' and 'sim' functions, respectively). A sufficiently large number of iterations (i.e. 50,000) at a small learning rate were required to train the neural network. According to this identified class number, the system matrices $\mathscr{A}, \mathscr{B}, \mathscr{C}$, the controller gain matrix **K** and Kalman filter gain matrix **L** are recalled from the memory, which are stored a priori. The controller again works for $\Re$ number of points without any identification/classification involved. When the iteration counter exceeds $\Re$, identification/classification takes place once again. In this way the adaptive controller continues to work until shutdown is requested.

6. Results and discussion

6.1. Neural Networks-based approach

Table 5 gives the CL response of the system obtained experimentally for the adaptive, as well as non-adaptive, controllers. According to the length $\Re$ of the data points used for updating the system parameters, different results were observed. These are discussed in detail as below.

6.1.1. Data length is 512 points

For the purpose of brevity all the figures showing the results, corresponding to different tip loads and different length of data series are not presented. However, Table 5, gives the required data. In this case $\Re$ is

Table 5
Table showing the comparison of various performance parameters for Neural Networks-based adaptive control and without control

Tip load (g)	Open loop settling time (s)	Non-adaptive control					Adaptive control					
		Settling time (s)	Modal amplitude (dB)				Length of data (L)	Settling time (s)	Modal amplitude (dB)			
			Sensor 1		Sensor 2				Sensor 1		Sensor 2	
			Mode 1	Mode 2	Mode 1	Mode 2			Mode 1	Mode 2	Mode 1	Mode 2
10	4.3	2.43	220	58	2000	0.0	512	1.45	57	8	460	0
							256	2.10	115.0	14.0	995.0	0.0
20	5.7	5.10	120	3.0	905	0.0	512	3.13	45	0	225	0
							256	3.20	102	7.0	610	0

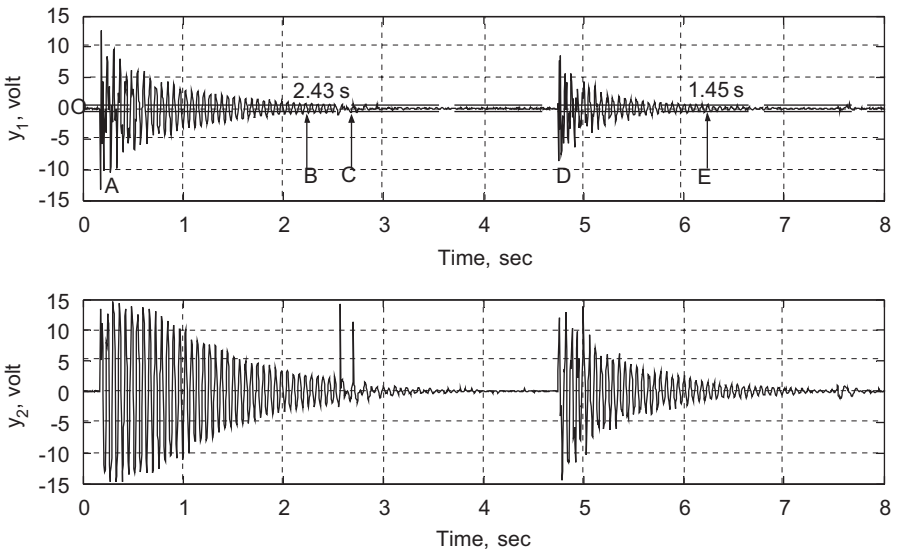

Fig. 8. Time domain responses by adaptive and non-adaptive control techniques with 10 g tip load and length of data series as 512 points.

taken as 512. The payload changes from 2 to 10 g. Fig. 8 shows the time domain response of the structure with 10 g tip load using the controller and observer designed for 2 g. In this figure, the response of the system to both the adaptive control (AC) and non-adaptive control (NAC) strategies is presented. By default the program's controller is set for 2 g tip load. As the system is excited, the controller designed for 2 g tip load is applied to the system. Since the data length for identification is of 512 point, which pertains to a time period of 2.56 s corresponding to a sampling rate of 200 Hz. With the NAC, a settling time of 2.43 s is obtained at point B. The OL settling time is 4.3 s. The controller starts at point O. At point C, at nearly 2.56 s, the controller stops and updates itself. Now the updated controller is pertaining to 10 g based on the frequencies obtained from stored data. At the point D the system is again excited from its equilibrium position. Since system has been updated, a settling time of 1.45 s is now obtained. With non-adaptive controller, modal amplitudes reduces to 220 and 58 dB at sensor 1 for the first and second mode, respectively. The modal amplitude for the first mode at sensor 2 by NAC is 2000 dB. Using AC modal amplitudes at sensor 1 reduce to 57 and 8 dB at first and second mode, respectively. Similarly, using AC, the first modal amplitude at sensor 2 reduces to 460 dB.

With NAC maximum amplitude of control voltages was 24 and 60 V at actuators 1 and 2, respectively, Fig. 9. Using AC this amplitude raises to 34 and 70 V at actuators 1 and 2, respectively. Due to this higher

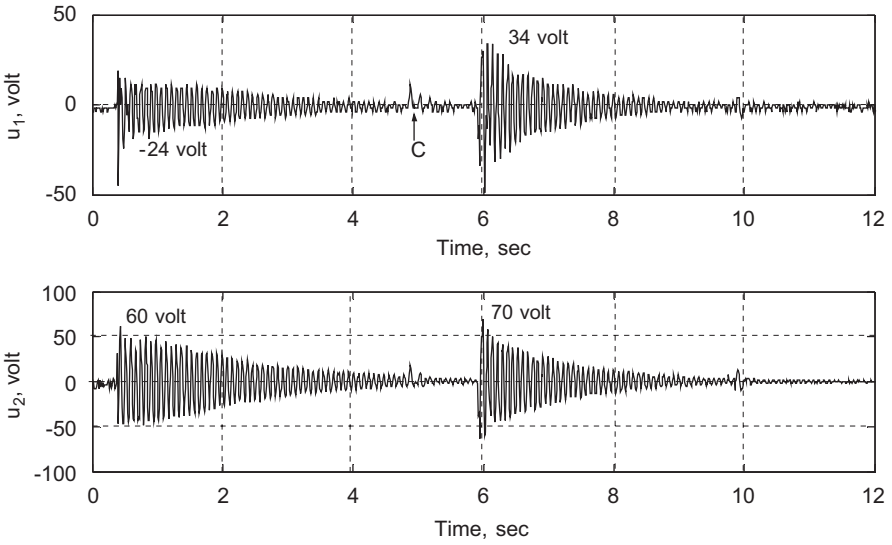

Fig. 9. Applied actuator voltages by adaptive and non-adaptive control techniques with 10 g tip load and length of data series as 512 points.

magnitude and proper phase of control voltage, CL settling time decreases. However, very high voltages can cause electrical breakdown of the piezoelectric materials. The breakdown occurs in the range 1800–2000 V [35]. Working at lower voltages results in increased life of the PZT actuators. In the present work much less voltages are applied.

Similarly, the controller is tested for a tip load from 2 to 20 g. NAC settling time was 5.1 s. The OL settling time is 5.3 s. Using AC, this settling time reduces to 3.13 s. Similarly, with NAC, maximum amplitudes of control voltages were 30 and 50 V at actuators 1 and 2, respectively. Using AC these amplitudes rise to 35 and 68 V at actuators 1 and 2, respectively.

6.1.2. *Data length is 256 points*

In this case, it was observed experimentally that the data length of 256 points is sufficient to find accurately the first few natural frequencies to the required accuracy. This means that controller updating will now take place after (256/200 = 1.28 s). In this case, the payload was changed from 2 to 20 g. The response time history is shown in Fig. 10. At point O, the controller starts. At point A, system is excited. From point A to point B the NAC pertaining to 2 g tip load is in action. At point B, controller updating takes place and the system is updated on the basis of natural frequencies calculated. At point B the non-updated controller (corresponding to 2 g tip load) stops for few milliseconds and controller updating takes place. At this point *the control action pauses for a while, and the structure tends to vibrate freely, causing a sudden shoot up of sensor voltage at point B.* The modal amplitude for the first mode at sensor 1 reduces to 102 dB instead of 45 dB with 512 data points discussed in Section 6.1 (Table 5). Also the modal amplitude for the first mode at sensor 2 reduces to 610 dB instead of 225 dB with 512 data points in the previous section (Table 5). The reason for this discrepancy is the addition of the affect of first 256 point starting from point A. During this period the NAC was in action, which contributes to some degradation of control properties. Still data length of 256 points is beneficial because, one need not wait for 512 points of poor performance, and then improves the system for better performance. The controller starts from a peak voltage of 12 V at actuator no. 1 and 50 V at actuator no. 2 for the first 256 points. Then controller updates and the control peak voltages shifts to 28 V at actuator no. 1 and to 50 V at actuator no. 2 (Fig. 11).

It is clear from the data presented above that by decreasing the length of data series used for identification, control performance decreases, but at the same time it has certain advantages also, i.e. very less time is wasted in non-adaptive time intervals. System performance improves rapidly. This may be attributed to the fact that, at lower value of data length, identification frequency increases. At more number of time instants,

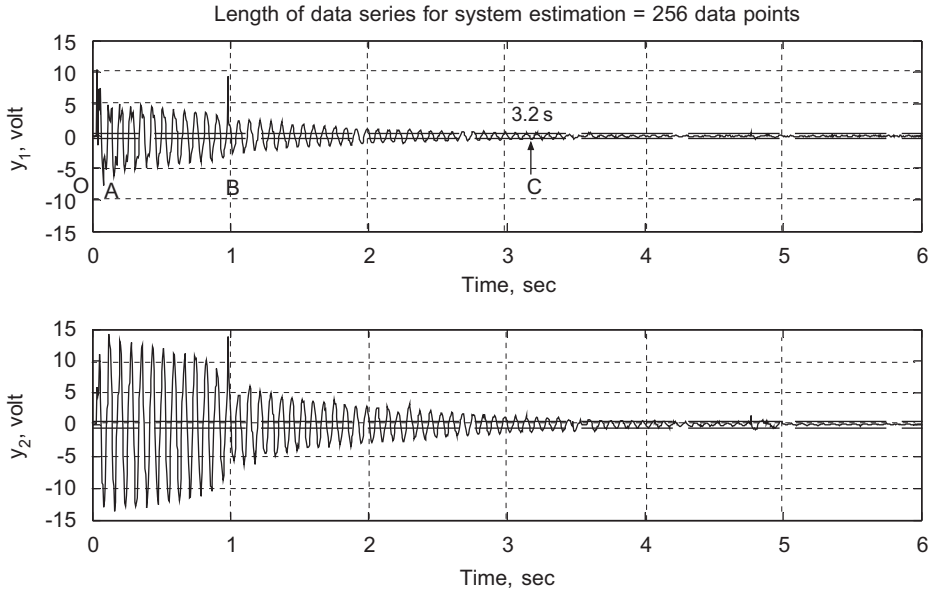

Fig. 10. Time domain response adaptive and non-adaptive control techniques with 20 g tip load and length of data series as 256 points.

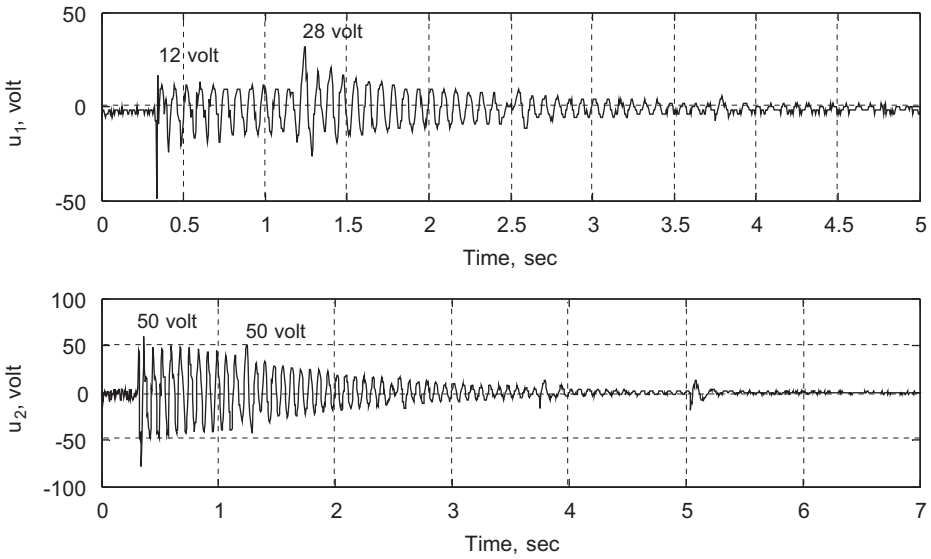

Fig. 11. Applied actuator voltages by adaptive and non-adaptive control techniques with tip load of 20 g and length of data series as 256 points.

identification takes place. During identification part, controller stops. When the controller stops, vibration amplitude suddenly increases. Hence the settling time as well as modal amplitudes remains at higher values.

6.2. Classical adaptive linear quadratic gaussian control approach

Afterward, adaptive linear quadratic gaussian (ALQG) control was tested. In this controller, system as well as controller parameters are updated keeping output and control weighing matrices fixed. As discussed in Section 3.3, *multivariable ALQG control is computational intensive, and hence requires devices running on real time operating systems. Lab VIEW-based real time engine is used to implement ALQG control*. Also, the stability problem associated with these adaptive control strategies is severe. In noise-dominated zones (i.e. at

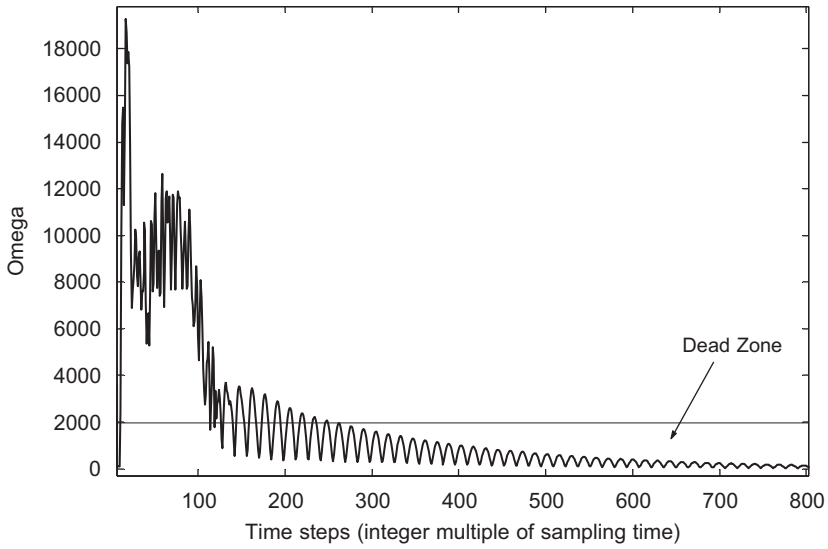

Fig. 12. Application of dead zone criterion for parameter adaptation.

low amplitudes where signal-to-noise ration is less), updating of system parameters is stopped [30]. To cope up the unmodeled disturbances (random vibrations) and the improper noise model, adaptation of system parameters is regulated. This regulation is done using the following criterion (to be used in Section 3.3):

$$\lambda_t = \begin{cases} 0 & \text{if } \omega_t^2 \leqslant \delta^2, \\ 1 & \text{otherwise.} \end{cases} \tag{24}$$

The scheduling variable ω_t can be calculated by using Ref. [30]. Fig. 12 shows the scheduling parameter ω_t as a function of amplitude. In the case of this dead zone-based approach, the system parameters modification stops in the dead zone because $\omega_t^2 \leqslant \delta^2$. The upper bond of the dead zone, δ is assumed to be known, which not a very hard assumption in case of random disturbances. Table 6 shows the performance parameters for a case when the ALQG controller was designed using the system parameters corresponding to 10 and 20 g loads. The output and control weighing matrices were kept fixed. The CL settling times were 2.20 and 3.50 s for tip loads 10 and 20 g, respectively. For tip load of 10 g, at sensor no. 1, the first and second mode amplitudes were 138 and 24 dB respectively. For tip load 20 g, corresponding amplitudes were 140 and 6 dB, respectively. Similar response was observed for sensor no. 2. So, to obtain better performance, the relative weight age of output and control weighing matrices must be changed. In classical ALQR design, there is no such provision for online change in relative weight age of control and output weighing matrices. So, even if modification of system or controller parameters is taking place online, desired performance cannot be obtained. However, from practical experience, this problem can be solved up to certain extent. But, using neural network-based technology; all these modifications are done offline. Hence CL system performs better than Adaptive LQR.

For the specific case in hand, by changing the relative weight age of output and control weighing matrices, better CL performance can be achieved. As the elements of control weighing matrix are increased in values, the performance is improved at sensor no. 1 and actuator no. 2 as shown in Fig. 13. Although, *the CL settling time is better* for different tip loads at sensor no. 1, *the transient response is quite poor*.

7. Conclusion

Smart robotic manipulators and machine structures with multimodal participation and multiple systems of actuators and sensors are considered for adaptive control in this work. An inverted L structure, which is a partial representative of these types of structures, is considered for study. As system parameters are changed, new system parameters are calculated on timely basis using system classification techniques. For these changed parameters, controller gains and observer gains were calculated offline by solving the Riccatti equation iteratively by changing the

Table 6
Table showing the effect of updating the controller parameters with fixing the output and control weighing matrices using Adaptive LQR

Tip load (g)	Closed loop settling time (s)	Closed loop modal amplitude (dB)			
		Sensor 1		Sensor 2	
		Mode 1	Mode 2	Mode 1	Mode 2
10	2.20	138	24	1050	0.0
20	3.50	140	6.0	793	6.0

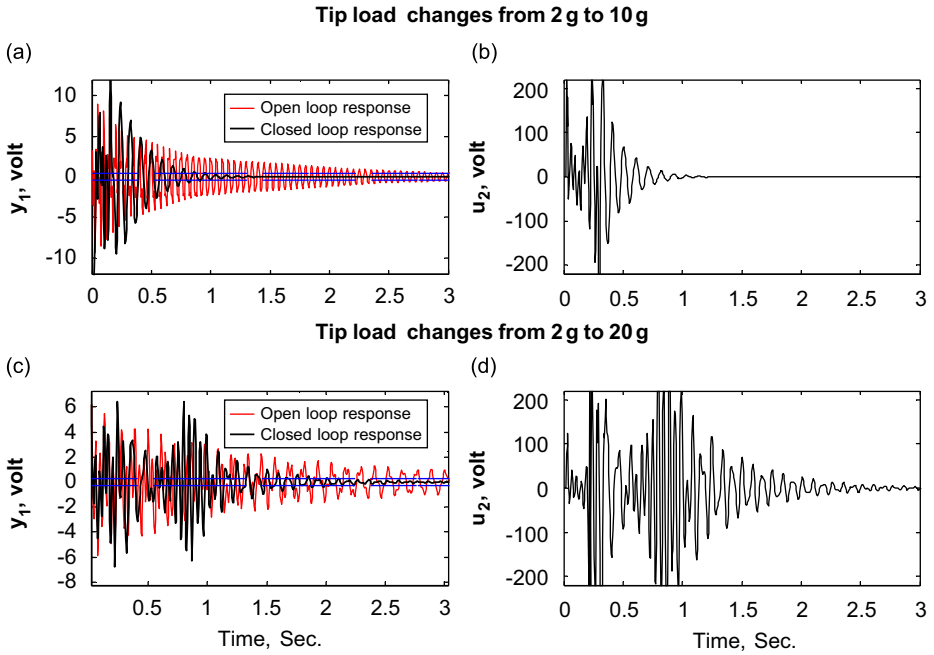

Fig. 13. Performance of classical adaptive LQG control with different tip load changes.

weight matrices. These system and controller parameters were saved and classified using learning vector quantization (LVQ) neural networks. These parameters were available during real time control by simulating the LVQ neural networks. The performance of the system improves drastically using re-identified system parameters and recalculated control and observer gains. The effect of identification data length is studied and the results point out that this data length should be judiciously chosen to have regular and accurate identification. When the results were compared with classical adaptive linear quadratic Gaussian controller, it was observed that better transient performance could be achieved by using system classification techniques. Also, these classical controllers are computation intensive and require specialized hardware. However, proposed controller can be implemented on a normal P-4 processor.

Appendix

A.1. Transformation from state-space form to difference equation form

The state-coupling matrix $\mathscr{A}$ and the input-coupling matrix $\mathscr{B}$ are denoted by

$$\mathscr{A} = \begin{bmatrix} 0 & 1 & 1 & 0 \\ a_{21} & a_{22} & a_{23} & a_{24} \\ 0 & 0 & 0 & 1 \\ a_{41} & a_{42} & a_{43} & a_{44} \end{bmatrix} \text{ with } a_{11} = a_{13} = a_{14} = a_{31} = a_{32} = a_{33} = 0 \text{ and } a_{12} = a_{34} = 1, \tag{A.1a}$$

$$\mathscr{B} = \begin{bmatrix} b_{11} & b_{12} \\ b_{21} & b_{22} \\ b_{31} & b_{32} \\ b_{41} & b_{42} \end{bmatrix}. \tag{A.1b}$$

The difference equation auro-regressive coefficient matrices $\mathbf{A}_0$, $\mathbf{A}_1$ and $\mathbf{A}_2$ are obtained from state coupling matrix $\mathbf{A}$ [26,27]:

$$\mathbf{P}_0 = \begin{bmatrix} 1 & 0 \\ 0 & 1 \end{bmatrix}, \quad \mathbf{P}_1 = \begin{bmatrix} -a_{33} & -a_{34} \\ -a_{43} & -a_{44} \end{bmatrix}, \quad \mathbf{P}_2 = \begin{bmatrix} -a_{11} & -a_{12} \\ -a_{21} & -a_{22} \end{bmatrix}. \tag{A.2}$$

The difference equation moving average coefficient matrices $\mathbf{Q}_1$ and $\mathbf{Q}_2$ are obtained by transformation matrix $\mathbf{M}$ is given by

$$\mathbf{M} = \begin{bmatrix} -a_{33} & 1 & -a_{34} & -a_{12} \\ 1 & 0 & -a_{12} & 0 \\ -a_{43} & -a_{21} & -a_{44} & 1 \\ -a_{21} & 0 & 1 & 0 \end{bmatrix}. \tag{A.3}$$

For obtaining $\mathbf{Q}_1$ and $\mathbf{Q}_2$ we have

$$\mathbf{Q}' = \mathbf{M}\mathbf{Q}, \tag{A.4}$$

$$\mathbf{Q}' = \begin{bmatrix} b'_{11} & b'_{12} \\ b'_{21} & b'_{22} \\ b'_{31} & b'_{32} \\ b'_{41} & b'_{42} \end{bmatrix} \tag{A.5}$$

and the moving average coefficient matrices are given by

$$\mathbf{Q}_1 = \begin{bmatrix} b'_{21} & b'_{22} \\ b'_{41} & b'_{42} \end{bmatrix}, \quad \mathbf{Q}_2 = \begin{bmatrix} b'_{11} & b'_{12} \\ b'_{31} & b'_{32} \end{bmatrix}. \tag{A.6}$$

A.2. Transformation from difference equation form to state-space form

The ARMA difference equation forms can be converted to Canonical State-Space form, which are suitable for control applications like Kalman Filter Design and Controller Design. Using certain transformation [26,27], the system matrices $\mathscr{A}$, $\mathscr{B}$ and $\mathscr{C}$ are easily calculated.

If $\mathbf{P_0}$, $\mathbf{P_1}$ and $\mathbf{P_2}$ are the auto-regressive coefficients and $\mathbf{Q_1}$ and $\mathbf{Q_2}$ are in moving average coefficients in matrix form,

$$\mathbf{P}_0 = \begin{bmatrix} 1 & 0 \\ 0 & 1 \end{bmatrix}, \quad \mathbf{P}_1 = \begin{bmatrix} p^1_{11} & p^1_{12} \\ p^1_{21} & p^1_{22} \end{bmatrix}, \quad \mathbf{P}_2 = \begin{bmatrix} p^2_{11} & p^2_{12} \\ p^2_{21} & p^2_{22} \end{bmatrix}, \tag{A.7a}$$

$$\mathbf{Q}_1 = \begin{bmatrix} q^1_{11} & q^1_{12} \\ q^1_{21} & q^1_{22} \end{bmatrix}, \quad \mathbf{Q}_2 = \begin{bmatrix} q^2_{11} & q^2_{12} \\ q^2_{21} & q^2_{22} \end{bmatrix} \tag{A.7b}$$

the state-coupling matrix $\mathscr{A}$ is given by Guidorzi [26,27]

$$\mathscr{A} = \begin{bmatrix} 0 & 1 & 0 & 0 \\ -p^2 11 & -p^1 11 & -p^2 12 & -p^1 12 \\ 0 & 0 & 0 & 1 \\ -p^2 21 & -p^1 21 & -p^2 22 & -p^1 22 \end{bmatrix}. \tag{A.8}$$

The coefficients of the input coupling matrix can be defined from the elements of the moving average matrices.

The first transformation to the transformation matrix $\mathscr{B}'$ is given as [26,27]

$$\mathscr{B}' = \begin{bmatrix} \ell'_{11} & \ell'_{12} \\ \ell'_{21} & \ell'_{22} \\ \ell'_{31} & \ell'_{32} \\ \ell'_{41} & \ell'_{42} \end{bmatrix} = \begin{bmatrix} \mathbf{Q}_2(1,1) & \mathbf{Q}_2(1,2) \\ \mathbf{Q}_1(1,1) & \mathbf{Q}_1(1,2) \\ \mathbf{Q}_2(2,1) & \mathbf{Q}_2(2,2) \\ \mathbf{Q}_1(2,1) & \mathbf{Q}_1(2,2) \end{bmatrix} = \begin{bmatrix} q_{11}^2 & q_{12}^2 \\ q_{11}^1 & q_{12}^1 \\ q_{21}^2 & q_{22}^2 \\ q_{21}^1 & q_{22}^1 \end{bmatrix} \tag{A.9}$$

where $\mathbf{Q}_1$ and $\mathbf{Q}_2$ are the moving average coefficients in matrix form. The other transformation matrix $\mathbf{N}$ is created using

$$\mathbf{N} = \begin{bmatrix} p_{11}^1 & 1 & p_{12}^1 & p_{12}^2 \\ 1 & 0 & p_{12}^2 & 0 \\ p_{21}^1 & p_{21}^2 & p_{22}^1 & 1 \\ p_{21}^2 & 0 & 1 & 0 \end{bmatrix}. \tag{A.10}$$

The input coupling matrix $\mathscr{B}$ is obtained by the following relation:

$$\mathscr{B} = \mathbf{N}^{-1}\mathscr{B}' \tag{A.11}$$

A.3. Transformation from difference equation form to matrix description form

If the difference equation coefficients (in matrix form) are given by

$$\mathbf{P}_0 = \begin{bmatrix} 1 & 0 \\ 0 & 1 \end{bmatrix}, \quad \mathbf{P}_1 = \begin{bmatrix} p_{111} & p_{112} \\ p_{121} & p_{122} \end{bmatrix}, \quad \mathbf{P}_2 = \begin{bmatrix} p_{211} & p_{212} \\ p_{221} & p_{222} \end{bmatrix},$$

$$\mathbf{Q}_1 = \begin{bmatrix} q_{111} & q_{112} \\ q_{121} & q_{122} \end{bmatrix}, \quad \mathbf{Q}_2 = \begin{bmatrix} q_{211} & q_{212} \\ q_{221} & q_{222} \end{bmatrix}$$

the matrix description form (MFD) of the system can be written as

$$\mathbf{Ay(t)} = \mathbf{Bu(t)} \tag{A.12}$$

such that

$$\begin{bmatrix} 1 + p_{111}z^{-1} + p_{211}z^{-2} & p_{112}z^{-1} + p_{212}z^{-2} \\ p_{121}z^{-1} + p_{221}z^{-2} & 1 + p_{122}z^{-1} + p_{222}z^{-2} \end{bmatrix} \begin{Bmatrix} y_1(t) \\ y_2(t) \end{Bmatrix} = \begin{bmatrix} q_{111}z^{-1} + q_{211}z^{-2} & q_{112}z^{-1} + q_{212}z^{-2} \\ q_{121}z^{-1} + q_{221}z^{-2} & q_{122}z^{-1} + q_{222}z^{-2} \end{bmatrix} \begin{Bmatrix} u_1(t) \\ u_2(t) \end{Bmatrix}, \tag{A.13}$$

where z^{-1} is the delay operator. Similarly the MFD form can be transformed to difference equation form.

References

[1] A.P. Tzes, S. Yurkowich, A frequency domain identification scheme for flexible structure control, *International Journal of Dynamic Systems Measurement and Control* 112 (1990) 427–434.
[2] A.P. Tzes, S. Yurkowich, Application and comparison of on-line identification methods for flexible manipulator control, *International Journal of Robotic Research* 10 (1991) 515–527.
[3] Y. Zeng, Araujo, S.N. Singh, Output feedback variable structure adaptive control of a flexible spacecraft, *Astronautica* 44 (1999) 11–22.
[4] S.H. Youn, J.H. Han, I. Lee, Neuro-adaptive vibration control of composite beams subjected to sudden de-lamination, *Journal of Sound and Vibration* 238 (2000) 215–231.
[5] J. Shaw, Adaptive control for sound and vibration: a comparative study, *Journal of Sound and Vibration* 235 (2000) 671–684.
[6] K.H. Rew, Multi-modal vibration control using adaptive positive position feedback, *Journal of Intelligent Materials and Structures* 13 (2002) 13–22.
[7] M.R. Bai, Experimental evaluation of adaptive predictive control for rotor vibration suppression, *IEEE Transactions on Control System Technology* 10 (2002) 895–901.
[8] C.W. Lim, T.Y. Chung, S.J. Moon, Adaptive bang-bang control for the vibration control of structures under earthquakes, *Earthquake Engineering and Structural Dynamics* 32 (2003) 1977–1994.
[9] X. Bu, L. Ye, Z. Su, C. Wang, Active control of flexible smart beam using system identification technique based on ARMAX, *Journal of Smart Materials and Structures* 12 (2003) 845–850.
[10] K.-J. Yuang, K.S. Keum Shik Hong, F. Matsuno, *Robust adaptive boundary control of an axially moving string under a spatiotemporally varying tension* 273 (2004) 1007–1029.
[11] C.F. Cutforth, L.Y. Pao, Adaptive input shaping for maneuvering flexible structures, *Automatica* 40 (2004) 685–693.
[12] M.B. Xu, G. Song, Adaptive control of vibration wave propagation in cylindrical shells using SMA wall joint, *Journal of Sound and Vibration* 278 (2004) 307–326.
[13] R. Kumar, S.P. Singh, H.N. Chandrawat, Multivariable adaptive vibration control of smart structures using iterative (LQG) control strategies, *Journal of Smart Materials and Structures* 14 (2005) 953–962.
[14] J.-C. Lin, M.H. Nien, Adaptive control of a composite cantilever beam with piezoelectric damping-modal actuators/sensors, *Composite Structures* 70 (2005) 170–176.
[15] R. Kumar, S.P. Singh, Adaptive hybrid control of smart structures subjected to multiple disturbances, *Journal of Smart Materials and Structures* 15 (2006) 1345–1357.
[16] R. Kumar, S.P. Singh, Adaptive vibration control of smart structures: a comparative study, *Journal of Smart Materials and Structures* 15 (2006) 1358–1369.
[17] L.-Q. Chen, W. Zhang, Adaptive vibration reduction of an axially moving string via a tensioner, *International Journal of Mechanical Sciences* 48 (2006) 1409–1415.
[18] G.B. Maganti, S.N. Singh, Simplified adaptive control of an orbiting flexible spacecraft, *Acta Astranautica* 61 (7–8) (2007) 575–589.
[19] X. Song, M. Ahmadin, Steve southward and lane miller, parametric study of non-linear adaptive control algorithm for magneto-rheological suspension systems, *Communications in Nonlinear Science and Numerical Simulations* 12 (2007) 584–607.
[20] R. Kumar, Adaptive pole placement techniques for active vibration control of smart structures: a feasibility study ASME Publication. *Journal of Vibration and Acoustics* (2007), accepted for publication ([VIB-06-1169] 020704 VAJ).
[21] Meirovitch, *Elements of Vibration Analysis*, McGraw-Hill Publishing Company, New York, 1986.
[22] Meirovitch, *Dynamics and Control of Structures*, Wiley, UK, 1986.
[23] S.S. Mohammed, A.R. Stubbered, G.H. Hostettler, *Digital Control System Design Saunders College Publishing*, Harcourt Brace College Publishers, Tokyo, 1994.
[24] R. Buttler, V. Rao, A state space modeling and control method for multivariable smart structural systems, *International Journal of Smart Materials and Structures* 5 (1996) 386–399.
[25] A. Baz, S. Poh, Performance of active control system with piezoelectric actuators, *International Journal of Sound and Vibration* 126 (1988) 327–343.
[26] R. Guidorzi, Canonical structures in the identification of multivariable systems, *Automatica* 11 (1975) 361–374.
[27] R. Guidorzi, Invariants canonical forms for structural and parametric identification, *Automatica* 17 (1981) 117–133.
[28] V. Kucera, *Discrete Linear Control: The Polynomial Equation Approach*, Wiley, New York, 1979.
[29] M.J. Grimble, Implicit and explicit LQG self-tuning controllers, *Automatica* 20 (1984) 661–669.
[30] R. Lozano, X.H. Zhao, Adaptive pole placement without excitation probing signals, *IEEE Transactions on Automatic Control* 39 (1994) 47–58.
[31] B. Kosko, *Neural Networks and Fuzzy Systems*, Prentice Hall of India, New Delhi, 1996.
[32] User Manual for MATLAB Toolbox for Neural Networks, MATHWORKS, 2005.
[33] User Manual for Virtual Instrumentation Software LAB VIEW, National Instruments, Austin, 2005.
[34] L. Ljung, *System Identification: Theory for the User*, Prentice Hall PTR, Upper Saddle River, NJ, 1999.
[35] H. Janocha, *Adaptronics and Smart Structures*, Springer, New York, 1999.